

## Article

# Effect of Arc Length on Oxygen Content and Mechanical Properties of Weld Metal during Pulsed GMAW

Jiachen Xu \*, Xiaoxiao Zhou and Dawei Zhu

College of Electrical Engineering, Nanjing Vocational University of Industry Technology, Nanjing 210023, China; 2018100948@niit.edu.cn (X.Z.); 2021101207@niit.edu.cn (D.Z.)

\* Correspondence: 2021101183@niit.edu.cn; Tel.: +86-025-8586-4060

**Abstract:** Pulsed gas metal arc weld (GMAW) was widely used for the advantages of controllable heat input, all-position welding, and no spatter. In order to obtain an ideal welding process, the stability of the arc length was studied in many researches, but the influence of arc length on the properties of weld metal was ignored. In this paper, the effect of arc length on oxygen content and mechanical properties of weld metal during pulsed GMAW was studied. Q690 high strength steel was selected as the base metal, and ER69-G solid wire, with a diameter of 1.2 mm, was used as the electrode wire. Additionally, the shielding gas and the wire feed rate were 82% Ar + 18% CO<sub>2</sub> and 4 m/min, respectively. The results showed that as the arc length raised from 2.9 mm to 9.2 mm, the oxidation reacted more completely in the droplet transfer zone, and the oxygen content of the weld metal increased significantly. The tensile strength of the weld metal reduced but the −40 °C impact energy heightened. Due to the longer arc, the proportion of acicular ferrite (AF) in the microstructure decreased, but the proportion of lath bainite (LB) and granular bainite (GB) decreased. The higher oxygen content of weld metal was useful for the formation of inclusions, which promoted the nucleation of acicular ferrite and dimples, contributing to the growth of plasticity and toughness of weld metal.

**Keywords:** arc length; oxygen content; mechanical properties; microstructure; weld metal



**Citation:** Xu, J.; Zhou, X.; Zhu, D. Effect of Arc Length on Oxygen Content and Mechanical Properties of Weld Metal during Pulsed GMAW. *Crystals* **2022**, *12*, 176. <https://doi.org/10.3390/cryst12020176>

Academic Editors: Fan Jiang, Mingxuan Yang and Pavel Lukáč

Received: 22 December 2021

Accepted: 21 January 2022

Published: 26 January 2022

**Publisher's Note:** MDPI stays neutral with regard to jurisdictional claims in published maps and institutional affiliations.



**Copyright:** © 2022 by the authors. Licensee MDPI, Basel, Switzerland. This article is an open access article distributed under the terms and conditions of the Creative Commons Attribution (CC BY) license (<https://creativecommons.org/licenses/by/4.0/>).

## 1. Introduction

With the development of industrial automation and robot welding, pulsed gas metal arc weld (GMAW) was widely used for the advantages of controllable heat input, all-position welding, and no spatter [1–3]. During the droplet transfer process in pulsed GMAW, “one droplet per pulse” (ODPP) was regarded as the most ideal mode [4–6], which was mainly affected by the pulse peak current ( $I_p$ ) and pulse peak current time ( $t_p$ ) [7–9]. In order to obtain a stable ODPP process, the pulse base current time ( $t_b$ ) was generally adjusted to change the arc length.

The shape of the arc, the heat transfer, and the heat dissipation mode of the droplets were greatly influenced by the arc length [10,11]. If the arc length were too short to provide sufficient space, the droplet would contact the molten pool but was still on the wire, contributing to a short circuit [12]. In addition, if the arc length were too long, the stability of the arc would decline and the oxidation reaction of liquid metal during the metal transfer process would be affected. However, the stability of the arc length was studied in many researches, while the effect of arc length on oxygen content and mechanical properties of weld metal was ignored [13,14].

In this paper, a high-speed camera was applied to investigate how the arc length affects the droplet transfer process. Additionally, by the analysis of the oxygen content and mechanical properties of weld metal, the relevant mechanism was discussed.

### 2. Experimental Method

In this paper, a synchronous acquisition system of high-speed photography, current, and voltage signal was used (shown in Figure 1). The welding torch was placed stationary over the workpiece on the platform and the high-speed camera system worked at 10,000 fps. In order to enhance the background brightness and magnify the contrast of images, a laser light with a wavelength of 850 nm was used as a backlight. Additionally, 20 mm thick Q690 high strength steel was selected as the base metal, and the butt joint was used. Thus, an ER69-G solid wire with a diameter of 1.2 mm was used as the electrode wire. Figure 2 shows the schematic diagram of welded joints and the selection of test specimens. The method of multi-layer multi-road welding was applied and the number of passes was 19, with a 6 mm thick backing plate under the weld. The preheating temperature before welding was controlled between 100 °C and 120 °C and the interpass temperature was controlled between 150 °C and 160 °C.

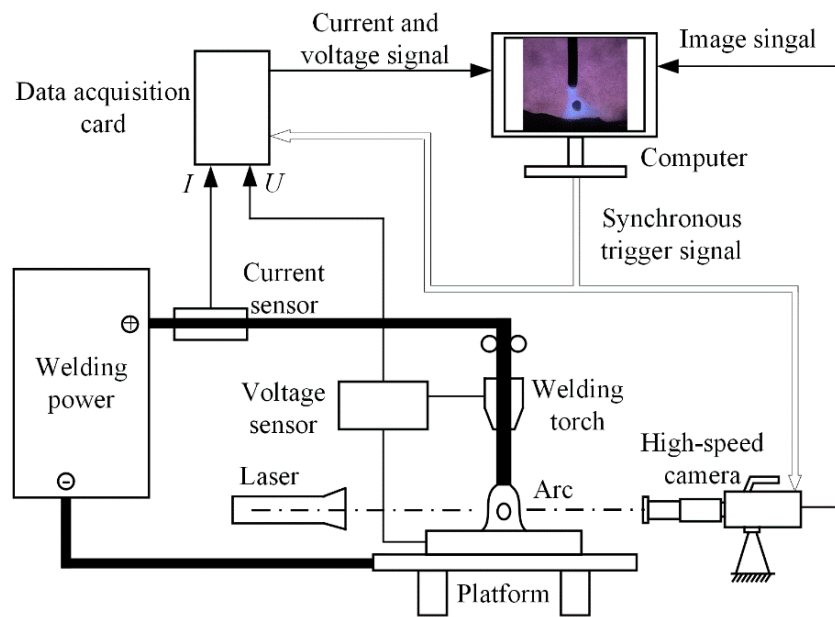


Figure 1. Schematic diagram of high-speed photography, current, and voltage signal synchronous acquisition system.

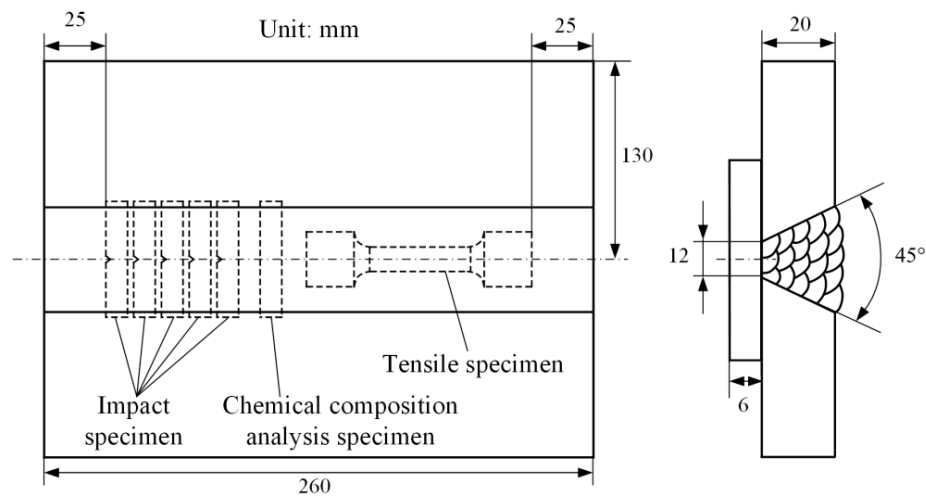


Figure 2. Schematic diagram of welded joints and selection of test specimens.

Table 1 shows the welding conditions. In order to obtain the ODPP droplet transfer mode, the pulse base current time was selected as the adjustable parameter to change the arc length.

**Table 1.** Welding conditions.

Welding Parameters	Test 1	Test 2	Test 3	Test 4
Contact tube-to-work distance, mm		20		
Pulse peak current, A		525		
Pulse peak current time, ms		1.6		
Pulse base current, A		28		
Pulse base current time, ms	9	8.2	7.4	6.6
Arc shielding gas		82% Ar + 18% CO <sub>2</sub>		
Flow rate of arc shielding gas, L·min <sup>-1</sup>		18		
Speed of wire feed, m·min <sup>-1</sup>		4		
Welding speed, mm·s <sup>-1</sup>		4		
Arc length, mm	2.9	4.5	6.5	9.2
Average current, A	122	130	139	149
Average voltage, V	22.4	25.9	28.1	31.3

The pulse base current time was 9, 8.2, 7.4, 6.6 ms from Test 1 to Test 4, respectively. The corresponding arc length was 2.9, 4.5, 6.5, 9.2 mm, respectively. The arc lengths were measured at the time of the maximum pulse peak current because the arc brightness was the largest and the boundary was clear at the moment.

According to the AWS B4.0-2016 standard [15], the impact specimens, the tensile specimen, and the chemical composition analysis specimen were cut out from the weld metal, as shown in Figure 2. The size of the standard impact specimen was 10 mm × 10 mm × 50 mm, with a 45° V-notch. The impact experiment was carried out at −40 °C. Figure 3 shows the detailed size of the tensile specimen. The tensile experiment was carried out at room temperature, during which the load speed was set as 1 mm·min<sup>-1</sup>. The metallographic samples of weld metal were cut from the center position perpendicular to the weld.

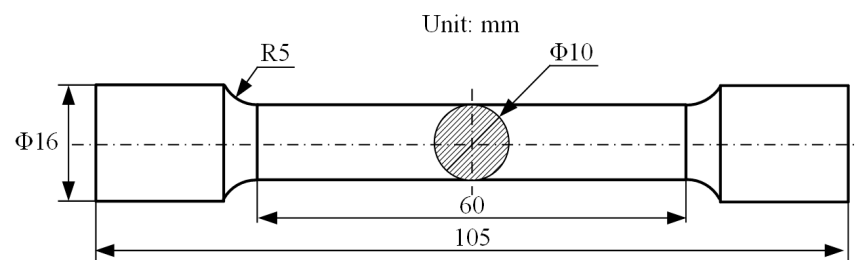


**Figure 3.** The size of the tensile specimen.

### 3. Results and Discussion

#### 3.1. Effect of Arc Length on Oxygen Content of Weld Metal

Figure 4 shows the oxygen content of weld metal under different arc lengths. As the arc length rises from 2.9 mm to 9.2 mm, the oxygen content increased by 71.4%, significantly from 217 ppm to 372 ppm. When the arc length was 4.5 mm and 9.2 mm, the oxygen content of weld metal was 235 ppm and 284 ppm, respectively.

The high-speed photographic images of droplets under different arc lengths are given in Figure 5. It can be seen that the mode of droplet transfer was ODPP, although the arc length was different. When the arc length was 2.9, 4.5, 6.5, 9.2 mm, the measured frequency of droplets was 94, 102, 111, and 122, respectively. Since the speed of wire feed remained unchanged in the experiments, the size of a single droplet would become smaller under the ODPP droplet transfer mode with the frequency of droplets rising, contributing that the specific surface area of liquid droplets increased and the metallurgical reaction between droplets and arc was strengthened. Moreover, the speed of the droplet slowed down with

the rise of arc length and the time of the droplet passing through the high-temperature arc increased from Figure 5. Therefore, the intensity and duration of an oxidation reaction in the whole droplet reaction zone increased, as well as the oxygen content of droplets. Finally, the oxygen element was transferred into the weld pool through the droplets, resulting in the increase of the oxygen content of the weld metal.

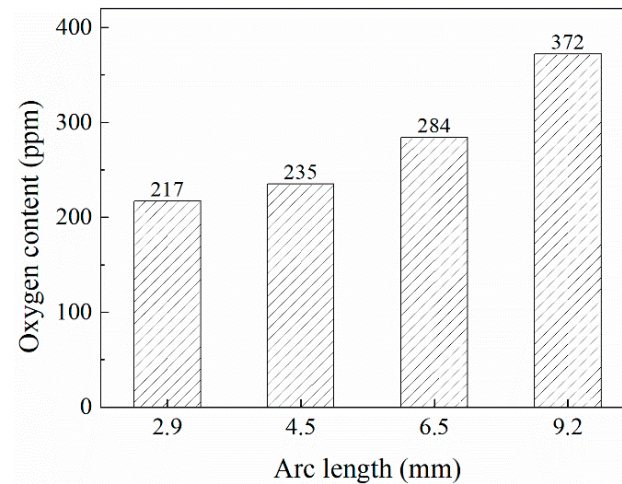


Figure 4. Oxygen content of weld metal under different arc lengths.

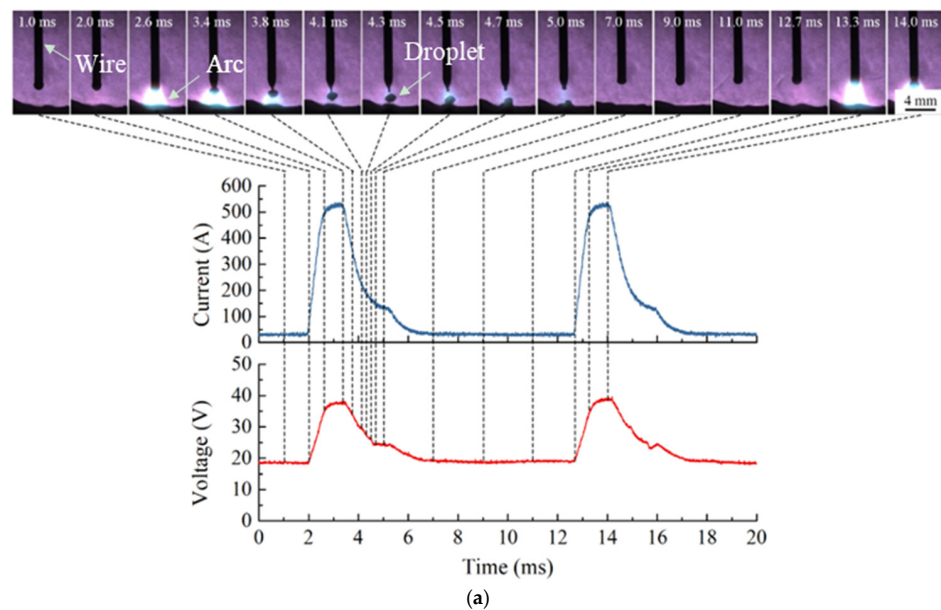
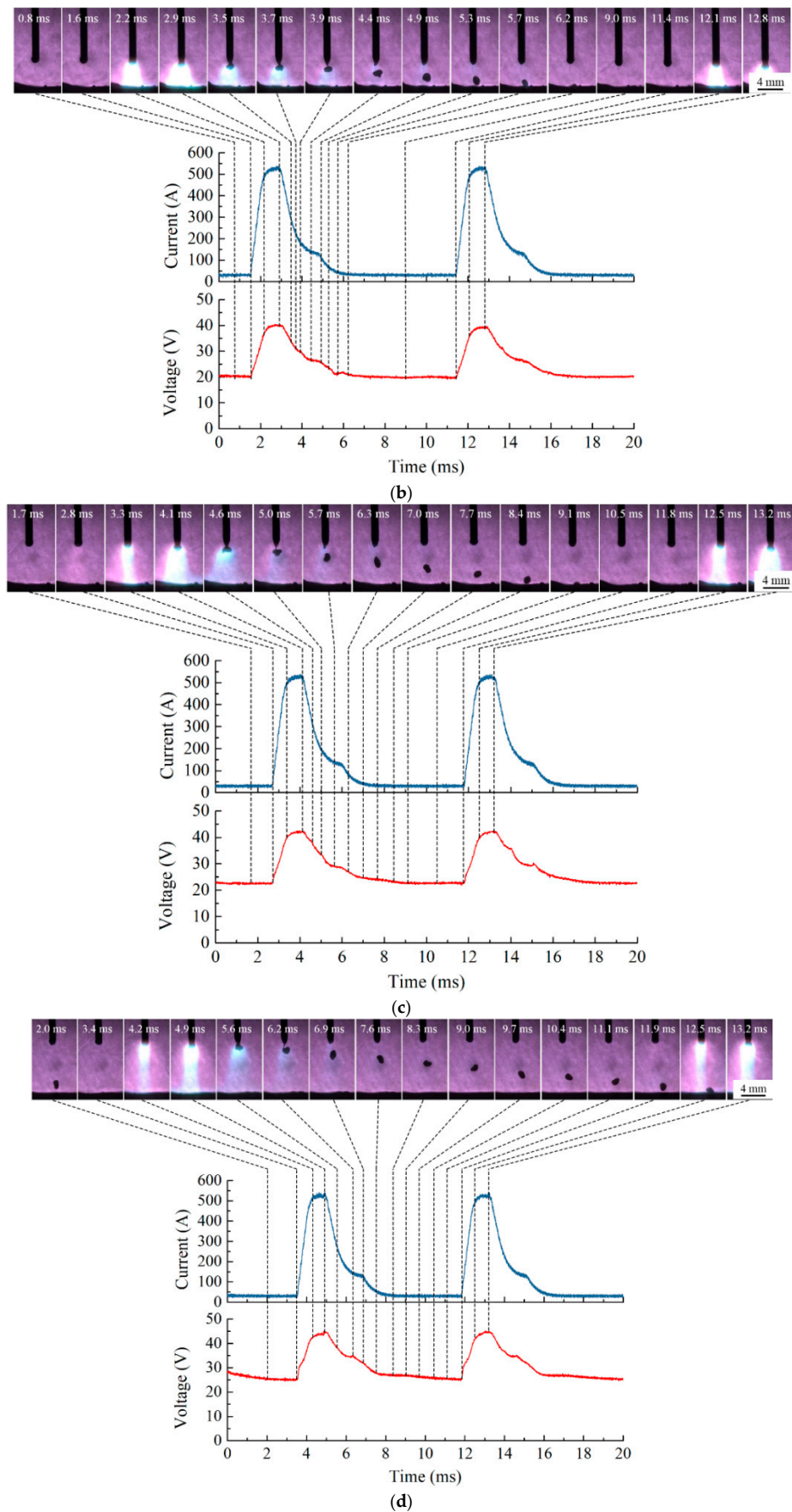


Figure 5. Cont.



**Figure 5.** High-speed photographic images of droplets under different arc lengths. Arc length: (a) 2.9 mm; (b) 4.5 mm; (c) 6.5 mm; (d) 9.2 mm.

### 3.2. Effect of Arc Length on Mechanical Properties of Weld Metal

The mechanical properties of weld metal were given in Figures 6 and 7. It can be seen that the tensile strength and yield strength of weld metal both gradually decreased with the rise of arc length, but the  $-40\text{ }^{\circ}\text{C}$  impact energy and the elongation rose. As the arc length grew from 2.9 mm to 9.2 mm, the tensile strength decreased from 781 MPa to 729 MPa and the  $-40\text{ }^{\circ}\text{C}$  impact energy increased from 79 J to 116 J.

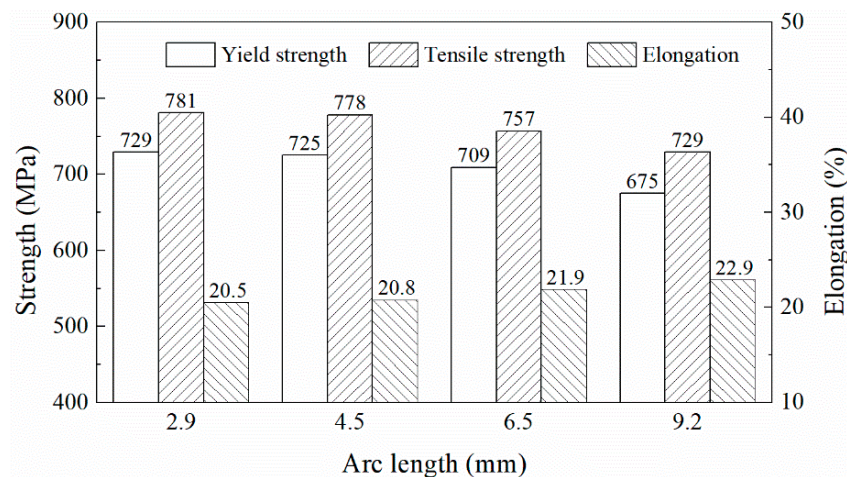


Figure 6. Tensile properties of weld metal under different arc lengths.

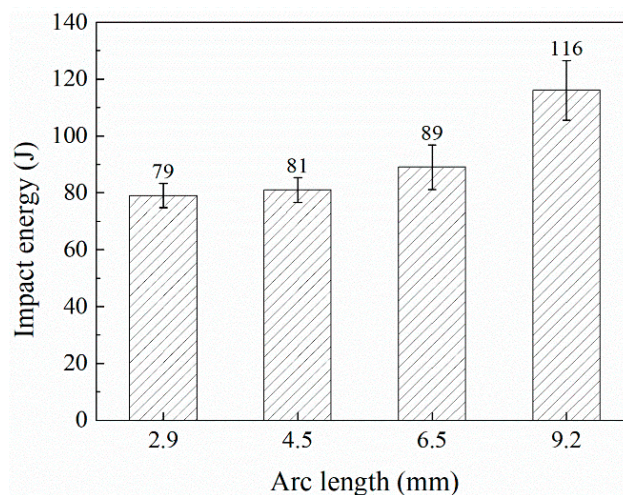


Figure 7.  $-40\text{ }^{\circ}\text{C}$  impact energy of weld metal under different arc lengths.

The chemical composition of weld wire is shown in Table 2. With the increase of arc length, the content of various alloy elements in the weld metal showed a decreasing trend, as given in Table 3. It can be seen that the decrease of alloy elements' content was related to the increased oxygen content. With the increase in arc length, the oxidation reaction of the droplets was enhanced, resulting in a more serious burning loss of metal alloy elements of welding wire. Therefore, the tensile strength was the largest under the shortest arc length (781 MPa) and the smallest (729 MPa) under the longest arc length.

Table 2. Chemical composition of weld wire (wt.%).

C	Si	Mn	Cu	Cr	Ni	Mo	Al	Ti
0.073	0.59	1.62	0.25	0.09	1.78	0.033	0.028	0.023

**Table 3.** Chemical composition of weld metal under different arc lengths (wt.%).

Arc Length $L_a$ /mm	C	Si	Mn	Cu	Cr	Ni	Mo	Al	Ti
2.9	0.063	0.47	1.51	0.19	0.07	1.71	0.029	0.017	0.017
4.5	0.062	0.46	1.49	0.18	0.06	1.71	0.029	0.016	0.016
6.5	0.053	0.41	1.42	0.16	0.04	1.66	0.026	0.009	0.009
9.2	0.047	0.38	1.37	0.13	0.02	1.61	0.022	0.006	0.007

From the metallographic microstructure (shown in Figure 8), it can be seen that the weld metal consisted of acicular ferrite (AF), lath bainite (LB), and granular bainite (GB). When the arc length was 2.9 mm, an obvious LB microstructure can be found, which was the strengthening phase. Therefore, the highest tensile strength can be obtained. When the arc length reached 9.2 mm, the microstructure of the weld metal was mainly AF, but LB can hardly be found. At the same time, GB became finer and more dispersed. The AF grains were fine and cross-distributed at a large angle, which divided the original austenite structure and can hinder the crack propagation, belonging to the toughening phase. When the microcrack propagated, it had to overcome the obstacle of a large number of AF, contributing to the greater  $-40\text{ }^\circ\text{C}$  impact energy of weld metal.

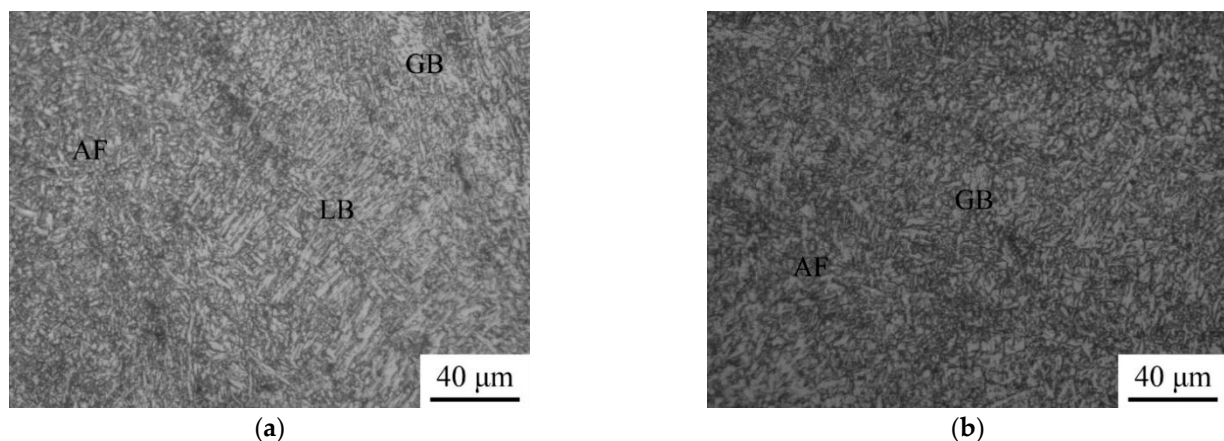
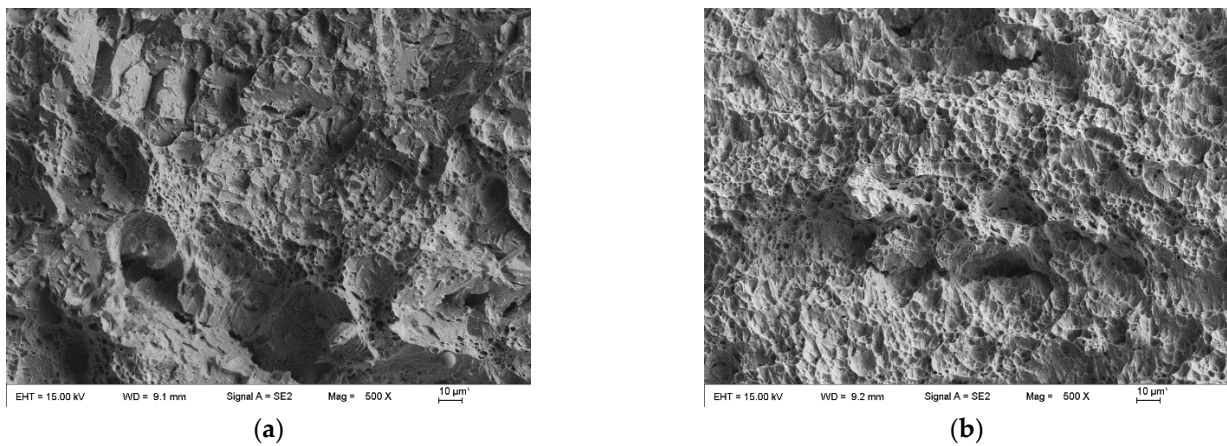
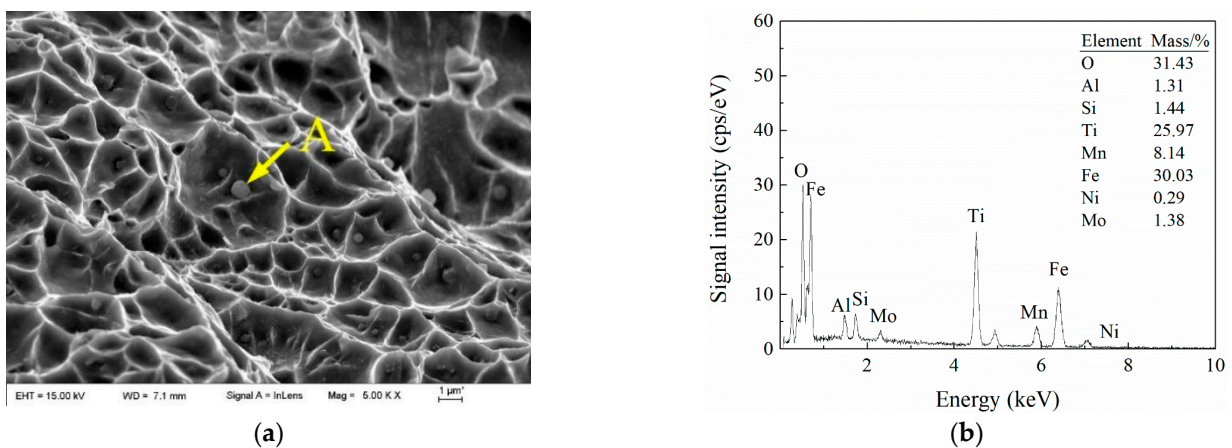
**Figure 8.** Metallographic microstructure of weld metal under different arc lengths. Arc length: (a) 2.9 mm; (b) 9.2 mm.

Figure 9 shows the impact of fracture morphology of weld metal under different arc lengths. Obvious cleavage steps but few dimples can be found when the arc length is 2.9 mm. When the plastic deformation was blocked, the stress in the local strong deformation area was relatively concentrated and the initiated crack expanded along the cleavage surface to release the stress, resulting in the cleavage steps. Cleavage steps were generally considered as being the characteristic morphology of brittle fracture. Therefore, the elongation and the  $-40\text{ }^\circ\text{C}$  impact energy were the lowest when arc length was 2.9 mm. When the arc length was 9.2 mm, most areas in the impact fracture were dimple morphology. The torn edge of the dimple was obvious and a few scattered cleavage steps were surrounded by a large number of dimples. As a result, better plasticity and toughness can be achieved.



**Figure 9.** Impact fracture morphology of weld metal under different arc lengths. Arc length: (a) 2.9 mm; (b) 9.2 mm.

Micromorphology using scanning electron microscope (SEM) and X-ray energy dispersion spectrometry (EDS) analysis result of inclusion in the dimple of impact fracture of weld metal is shown in Figure 10. It can be seen that spherical inclusions were found at the bottom of the dimples. According to the EDS analysis result, the inclusions were made from O, Al, Si, Ti, Mn, Fe, Ni, Mo, and other elements. Considering O element is not easy to combine with Ni and Mo, Ni, and Mo in the EDS analysis result may come from the base of weld metal. The inclusions of weld metal are often the compounds or composites formed by the combination of multiple elements. Therefore, it can be inferred that the inclusions may contain O, Al, Si, Ti, Mn, Fe, and other elements, and the oxides of the above elements (including  $\text{TiO}_2$ ,  $\text{SiO}_2$ ,  $\text{MnO}_2$ ,  $\text{Al}_2\text{O}_3$ ,  $\text{FeO}$ , and their composites) were the main components. In addition, with the rise of arc length, the oxygen content in weld metal increased, which indicated that the number of inclusions in the impact fracture also increased. Inclusions promoted the nucleation of acicular ferrite and dimples, contributing to the growth of plasticity and toughness of weld metal. A similar effect of the oxygen content on the microstructure and mechanical properties was also observed in Zhang's studies [16,17].



**Figure 10.** (a) SEM micromorphology of an area of dimples of impact fracture when arc length was 9.2 mm; (b) EDS analysis of point A in (a).

#### 4. Conclusions

The effect of arc length on oxygen content and mechanical properties of weld metal during pulsed GMAW was studied in this paper. The main conclusions can be summarized below:

- (1) As the arc length raised from 2.9 mm to 9.2 mm, the transfer time increased but the droplet size diminished. Meanwhile, the oxidation reacted more completely in the droplet transfer zone, and the oxygen content of the weld metal increased significantly from 217 ppm to 372 ppm.
- (2) When the arc length increased from 2.9 mm to 9.2 mm, the tensile strength of the weld metal reduced from 781 MPa to 729 MPa but the  $-40\text{ }^{\circ}\text{C}$  impact energy heightened from 79 J to 116 J.
- (3) Due to the longer arc, the proportion of AF in the microstructure decreased, but the proportion of LB and GB decreased. With the rise of arc length, the cleavage step morphology decreased in the impact fracture however, the dimples increased.
- (4) The more oxygen content of weld metal was useful for the formation of inclusions in impact fracture. Inclusions promoted the nucleation of acicular ferrite and dimples, contributing to the growth of plasticity and toughness of weld metal.

**Author Contributions:** Conceptualization, J.X.; methodology, X.Z. and D.Z.; software, J.X.; validation, J.X.; formal analysis, J.X.; investigation, J.X.; resources, J.X.; data curation, J.X.; writing—original draft preparation, J.X.; writing—review and editing, J.X.; visualization, J.X.; supervision, J.X.; project administration, J.X.; funding acquisition, J.X. All authors have read and agreed to the published version of the manuscript.

**Funding:** This project is supported by the introduction of a talent research start-up fund of Nanjing Vocational University of Industry Technology (Grant No. YK21-02-05).

**Institutional Review Board Statement:** Not applicable.

**Informed Consent Statement:** Not applicable.

**Data Availability Statement:** Not applicable.

**Acknowledgments:** The authors sincerely acknowledge the financial support by introduction of a talent research start-up fund of Nanjing Vocational University of Industry Technology, Grant No. YK21-02-05.

**Conflicts of Interest:** The authors declare no conflict of interest.

## References

1. Xu, Y.; Fang, G.; Lv, N.; Chen, S.; Zou, J.J. Computer Vision Technology for Seam Tracking in Robotic GTAW and GMAW. *Robot. Comput.-Integr. Manuf.* **2015**, *32*, 25–36. [[CrossRef](#)]
2. Xu, Y.; Lv, N.; Fang, G.; Du, S.; Zhao, W.; Ye, Z.; Chen, S. Welding Seam Tracking in Robotic Gas Metal Arc Welding. *J. Mater. Process. Technol.* **2017**, *248*, 18–30. [[CrossRef](#)]
3. Kozakov, R.; Gött, G.; Schöpp, H.; Uhrlandt, D.; Schnick, M.; Häföler, M.; Füssel, U.; Rose, S. Spatial Structure of the Arc in a Pulsed GMAW Process. *J. Phys. D Appl. Phys.* **2013**, *46*, 224001. [[CrossRef](#)]
4. Pal, K.; Pal, S.K. Effect of Pulse Parameters on Weld Quality in Pulsed Gas Metal Arc Welding: A Review. *J. Mater. Eng. Perform.* **2011**, *20*, 918–931. [[CrossRef](#)]
5. Ghosh, P.K.; Goyal, V.K.; Dhiman, H.K.; Kumar, M. Thermal and Metal Transfer Behaviours in Pulsed Current Gas Metal Arc Weld Deposition of Al–Mg Alloy. *Sci. Technol. Weld. Join.* **2006**, *11*, 232–242. [[CrossRef](#)]
6. Wu, C.S.; Chen, M.A.; Lu, Y.F. Effect of Current Waveforms on Metal Transfer in Pulsed Gas Metal Arc Welding. *Meas. Sci. Technol.* **2005**, *16*, 2459–2465. [[CrossRef](#)]
7. Amin, M. Pulse Current Parameters for Arc Stability and Controlled Metal Transfer in Arc Welding. *Met. Constr.* **1983**, *15*, 272–278.
8. Rajasekaran, S. Weld Bead Characteristics in Pulsed GMA Welding of Al–Mg Alloys. *Weld. J.* **1999**, *78*, 397s–407s.
9. Rajasekaran, S.; Kulkarni, S.D.; Mallya, U.D.; Chaturvedi, R.C. Droplet Detachment and Plate Fusion Characteristics in Pulsed Current Gas Metal Arc Welding. *Weld. J.* **1998**, *77*, 254s–269s.
10. Harwig, D.D.; Dierksheide, J.E.; Yapp, D.; Blackman, S. Arc Behavior and Melting Rate in the VP-GMAW Process. *Weld. J.* **2006**, *85*, 52s–62s.
11. Chen, C.; Fan, C.; Cai, X.; Lin, S.; Yang, C. Analysis of Droplet Transfer, Weld Formation and Microstructure in Al–Cu Alloy Bead Welding Joint with Pulsed Ultrasonic-GMAW Method. *J. Mater. Process. Technol.* **2019**, *271*, 144–151. [[CrossRef](#)]
12. Tong, H.; Ueyama, T.; Tanaka, M.; Ushio, M. Observations of the Phenomenon of Abnormal Arc Voltage Occurring in Pulsed Metal Inert Gas Welding of Aluminum Alloy. *Sci. Technol. Weld. Join.* **2005**, *10*, 695–700. [[CrossRef](#)]
13. Wang, Q.; Qi, B.; Cong, B.; Yang, M. Output Characteristic and Arc Length Control of Pulsed Gas Metal Arc Welding Process. *J. Manuf. Process.* **2017**, *29*, 427–437. [[CrossRef](#)]

14. Zhu, Z.; Wu, W.; Chen, Q. Random Nature of Droplet Size and Its Origins in Short Circuit CO<sub>2</sub> Arc Welding. *Sci. Technol. Weld. Join.* **2013**, *10*, 636–642. [[CrossRef](#)]
15. American Welding Society. *AWS B4.0-2016, Standard Methods for Mechanical Testing of Welds*; American National Standards Institute: Orlando, FL, USA, 2016.
16. Zhang, T.; Li, Z.; Kou, S.; Jing, H.; Li, G.; Li, H.; Kim, H.J. Effect of inclusions on microstructure and toughness of deposited metals of self-shielded flux cored wires. *Mater. Sci. Eng. A* **2015**, *628*, 332–339. [[CrossRef](#)]
17. Zhang, T.; Li, Z.; Ma, S.; Kou, S.; Jing, H. High strength steel (600–900 MPa) deposited metals: Microstructure and mechanical properties. *Sci. Technol. Weld. Join.* **2016**, *21*, 186–193. [[CrossRef](#)]